

Dynamical aspects of a bouncing ball in a nonhomogeneous field

Felipe Augusto O. Silveira ^{1,2}, Sidney G. Alves ¹, Edson D. Leonel,³ and Denis G. Ladeira^{1,*}

¹*Departamento de Estatística, Física e Matemática, UFSJ–Universidade Federal de São João del-Rei, Rod. MG 443, Km 7, Fazenda do Cadete, CEP: 36420-000, Ouro Branco, Minas Gerais, Brazil*

²*Programa de Pós-graduação em Física, UFSJ, Minas Gerais, Brazil*

³*Departamento de Física, UNESP–Universidade Estadual Paulista, Av. 24A, 1515 Bela Vista, CEP: 13506-900, Rio Claro, São Paulo, Brazil*



(Received 22 June 2020; revised 27 March 2021; accepted 12 May 2021; published 3 June 2021)

We study some dynamical properties of a charged particle that moves in a nonhomogeneous electric field and collides against an oscillating platform. Depending on the values of parameters, the system presents (i) predominantly regular dynamics or (ii) structures of chaotic behavior in phase space conditioned to the initial conditions. The localization of the fixed points and their stability are carefully discussed. Average properties of the chaotic sea are investigated under a scaling approach. We show that the system belongs to the same universality class as the Fermi-Ulam model.

DOI: [10.1103/PhysRevE.103.062205](https://doi.org/10.1103/PhysRevE.103.062205)

I. INTRODUCTION

Billiard dynamical systems are composed of a particle, or an ensemble of noninteracting particles, which collides against either static or time dependent boundaries as the time evolves [1–3]. For a fixed boundary, elastic collisions, and when the dynamics happens in conservative fields, the energy of the particle is preserved [4]. On the other hand, when the boundary is moving in time, the energy of the particle is no longer preserved and diffusion in the velocity of the particle may be observed, a condition that may lead to the phenomenon of Fermi acceleration [3,5]. Such a phenomenon is characterized by the unlimited growth of average energy for an ensemble of particles due to collisions with infinitely heavy and moving walls (boundary of the billiard). The bouncer model [6,7] is composed of a particle moving in a constant gravitational field and that collides with a platform moving with an angular frequency and a given amplitude. In this model, the control parameter is the dimensionless oscillation amplitude of the platform. Depending on the phase of the moving platform, the particle may gain or lose energy. Depending on the values of initial conditions and the control parameter, the model may exhibit a large variety of dynamical regimes. In the regime of low nonlinearity the bouncer model presents a phase space where regions of chaotic motion may be observed but are rather small. With the increase of the parameter controlling the nonlinearity, the chaotic portions observed in the phase space increase, always limited by a set of invariant spanning curves, until a critical limit where all the invariant spanning curves are destroyed. From such a limit any further increase of the control parameter leads to unlimited chaotic diffusion in phase space and hence to the observation of Fermi acceleration [8,9]. A careful discussion of this phenomenon was presented by Lichtenberg *et al.* [10] who demonstrated the equivalence of the bouncer model and the Chirikov Standard Map [11]. The model also presents an

interesting dynamical regime with the presence of accelerating modes, which lead the energy of the particles associated to regular orbits to show ballistic growth [11,12]. The bouncer model was studied in many different contexts and considering either conservative or nonconservative approaches [7,13–16], including quantum versions [17,18], experimental study [19], the bouncing of a hollow sphere partially filled with grains [20], scaling properties [21], application in atomic force microscopes, where the tip of the cantilever acts as a bouncing mass [22], crises events [23], the aspects of periodic dynamics [24,25], the influence of the accelerating modes in the transition from normal to ballistic diffusion in the bouncer model [26], the bouncing dynamics of small drops on liquid surface [27], thermodynamic aspects [28], and frequency-dependent diffusion coefficient [29].

In this paper we study a modification of the bouncer model where a charged particle is moving under a nonhomogeneous electric field. The system is made of a rigidly fixed sphere with a homogeneous charge distribution with a very thin aperture through which a dimensionless charged particle moves. The particle collides elastically with an oscillating platform placed in the aperture of the sphere. The position of the platform changes periodically in time. The nonlinearity is introduced in the motion of the particle due to the collisions with the moving platform. So far as we can tell, the present model is a specific example of a one-dimensional billiard experiencing elastic collisions and a linear restoring force. We obtain the equations that describe the dynamics of the system by using two dynamical variables, namely, the velocity of the particle and the phase of the moving platform at the instants of the collisions. We notice that, depending on combination of the parameters, the phase space presents (i) numerous regular orbits, periodic and quasiperiodic, including Kolmogorov-Arnold-Moser (KAM) islands around elliptical fixed points and spanning curves; or (ii) a mixed structure, composed of chaotic orbits, islands of regular motion, and invariant spanning curves. We conduct the numerical studies on the complete version of the model and we use the static wall approximation [30], also

*Corresponding author: dgl@ufsj.edu.br

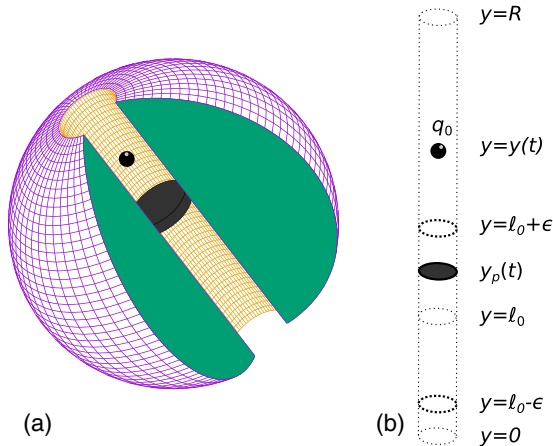


FIG. 1. (a) Illustration of the system showing the inner details and (b) the reference system used.

called the simplified version, to obtain some of the analytical results. We then identify the coordinates of the fixed points and discuss their classification with respect to stability. We describe the scaling properties of the system near the transition from the integrable regime to the nonintegrable regime. In order to obtain this scaling description, we focus on the low energy chaotic dynamics.

The paper is organized as follows. In the next section we describe the details of the system and construct the map that describes the dynamics of the particle. In Sec. III we discuss how the structure of phase space evolves as the parameters change. We present the scaling analysis in Sec. IV. Section V is dedicated to additional discussions and we draw the conclusions in Sec. VI.

II. THE MODEL

The system consists of a sphere of radius R with electric charge $-Q < 0$ uniformly distributed in its volume and a particle with charge $q_0 > 0$ and mass m . The particle moves in a very thin aperture that crosses the sphere through its center, as shown in Fig. 1(a). The restoring electric force points towards the center of the sphere and makes the position of the particle oscillate in time. An oscillating platform moves periodically in time t' with frequency ω and amplitude ϵ around the position located at a distance ℓ_0 from the center of the sphere. This is a prototype model that can be constructed in a laboratory and investigated experimentally.

Without loss of generality, we use the variable y to represent the charge and platform positions as shown in Fig. 1(b), where $y = 0$ is set in the center of the sphere. In this way, the platform moves in time according to the expression $y_p(t') = \ell_0 + \epsilon \cos(\omega t' + \phi_0)$, where ϕ_0 is an initial phase. The motion of the particle in the time interval between collisions with the moving platform is integrable and it is given by $y(t') = \varrho_n \cos(\omega_f t' - \delta_n)$, where ω_f is the frequency of oscillation of the particle due to the restoring force and it is given by $\omega_f^2 = q_0 Q / (4\pi \epsilon_0 R^3 m)$. Moreover, ϱ_n , the amplitude of oscillation of the particle, and δ_n are constants between collisions, and their values depend on the state of the system at the instant t'_n , as we describe below. At instant t'_n the particle collides against

the moving platform at position $y(t'_n) = y_p(t'_n)$ and acquires velocity v_n . The motion of the platform is not affected by the collision. Then the particle travels under action of the electric force and, after a time interval, another impact occurs against the platform.

Before we proceed, it is suitable to introduce some dimensionless quantities. The dimensionless time, positions and velocities are defined, respectively, by $t = \omega t'$, $Y = y/\ell_0$ and $V = v/(\omega \ell_0)$. The parameter $\epsilon = \epsilon/\ell_0$ is the dimensionless amplitude of oscillation of the platform. We define also the ratio of frequencies $\Omega = \omega_f/\omega$. In this way, a decrease in the value of parameter Ω can be thought as an increase in the frequency ω of oscillation of the platform, or it can be thought as a decrease in the absolute value of the charges or even an increase in the mass of the particle. We define the phase of the platform at an instant t by the expression $\phi = t + \phi_0$. So the n th impact occurs at position $Y_n = Y_p(\phi_n) = 1 + \epsilon \cos \phi_n$ and we obtain the two-dimensional map

$$\begin{aligned} Y_{n+1} &= \rho_n \Omega \sin[\Omega(\phi_{n+1} - \phi_0) - \delta_n] - 2\epsilon \sin \phi_{n+1}, \\ \phi_{n+1} &= \phi_n + \Delta t_{n+1}. \end{aligned} \quad (1)$$

In the equation above, Δt_{n+1} is the time interval between two collisions, $\rho_n = \rho(\phi_n, V_n)$ is the dimensionless amplitude of oscillation of the particle after the n th collision, and it is given by $\rho_n^2 = \varrho_n^2/\ell_0^2 = Y_n^2 + (V_n/\Omega)^2$. Moreover, $\delta_n = \delta(\phi_n, V_n)$ is given in terms of the expressions $o_n = \rho_n \cos \delta_n$ and $p_n = \rho_n \sin \delta_n$, where

$$\begin{aligned} o_n &= o(\phi_n, V_n) \\ &= Y_n \cos[\Omega(\phi_n - \phi_0)] - (V_n/\Omega) \sin[\Omega(\phi_n - \phi_0)], \\ p_n &= p(\phi_n, V_n) \\ &= Y_n \sin[\Omega(\phi_n - \phi_0)] + (V_n/\Omega) \cos[\Omega(\phi_n - \phi_0)]. \end{aligned} \quad (2)$$

The value of Δt_{n+1} in the map (1) is the smallest non-null solution obtained numerically from the transcendental equation below:

$$\begin{aligned} o_n \cos[\Omega(t_n + \Delta t_{n+1})] + p_n \sin[\Omega(t_n + \Delta t_{n+1})] \\ - 1 - \epsilon \cos(t_n + \Delta t_{n+1} + \phi_0) = 0. \end{aligned} \quad (3)$$

We provide the details needed to obtain the above equations in the Appendix. It is worth mentioning we are considering in this work the situations where the motion of the platform and particle are confined in the region $0 < 1 - \epsilon \leq Y < R/\ell_0$. The first inequality, $\epsilon < 1$, ensures a collision in a time interval smaller than half of the period of oscillation of the particle. The inequality $Y < R/\ell_0$ guarantees the particle is inside the sphere. Moreover, we do not take into account the dissipation of energy involved when electric charges are accelerated.

At the collisions instants the platform transfers energy and momentum to the particle. Depending on the phase of motion of the platform at the instant of collision, the particle may gain or lose energy. Moreover, there are situations where the velocity of the particle remains constant after each collision with the moving platform. The values of velocity of the particle and the phase of the platform for which this kind of equilibrium occurs are called fixed points. According to the stability, the fixed points are classified into two main

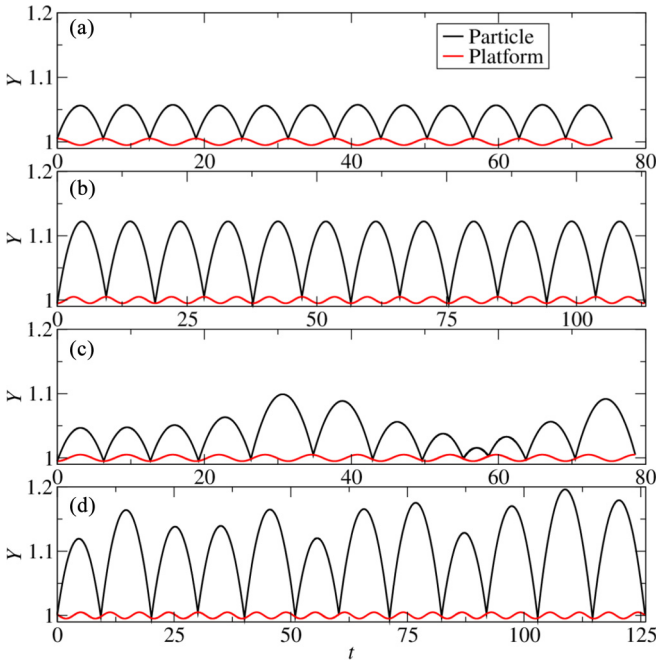


FIG. 2. Illustration of the positions of the platform and of the particle as functions of time. In (a) it is shown the orbits for an initial condition near a stable fixed point. (b) illustrates the orbits for an initial condition near a period-two trajectory. (c) exemplifies the situation where orbits start near an unstable fixed point. We present in (d) a case where the orbit of the particle is irregular. The values of parameters are $\epsilon = 5 \times 10^{-3}$ and $\Omega = 10^{-1}$.

classes: stable or unstable. A fixed point is stable when the orbit of an initial condition close to this fixed point remains near to the fixed point as the time goes on. On the other hand, a fixed point is unstable when the distance between the fixed point and the orbit of an initial condition close to the fixed point increases in time. Figure 2 illustrates the orbits of the platform (red curves) and of the particle (black curves) as functions of time for four situations. The points where the curves touch correspond to the instants of collisions. Between two collisions the motion of the particle is characterized by segments of cosine functions. Figure 2(a) illustrates the orbits for an initial condition near a stable fixed point. We see that one collision occurs at each oscillation of the platform, when the platform is near to its maximum position. We observe also that the motion of the particle exhibits a pattern where the amplitude of motion remains nearly the same after each collision. Figure 2(b) displays the orbits for an initial condition near a period-two orbit. A new collision occurs at each one-and-a-half oscillations of the platform, alternating between a minimum and a maximum position of platform, and the amplitude of motion of the particle is approximately the same after each collision against the platform. Figure 2(c) illustrates the orbits for an initial condition near an unstable fixed point. For the first few collisions we observe that the orbit of the particle remains nearly regular, with the collisions occurring at the instants where the platform is close to its lowest position. After that, the orbit of the particle becomes irregular. Depending on the values of parameters and initial conditions the particle acquires an apparently er-

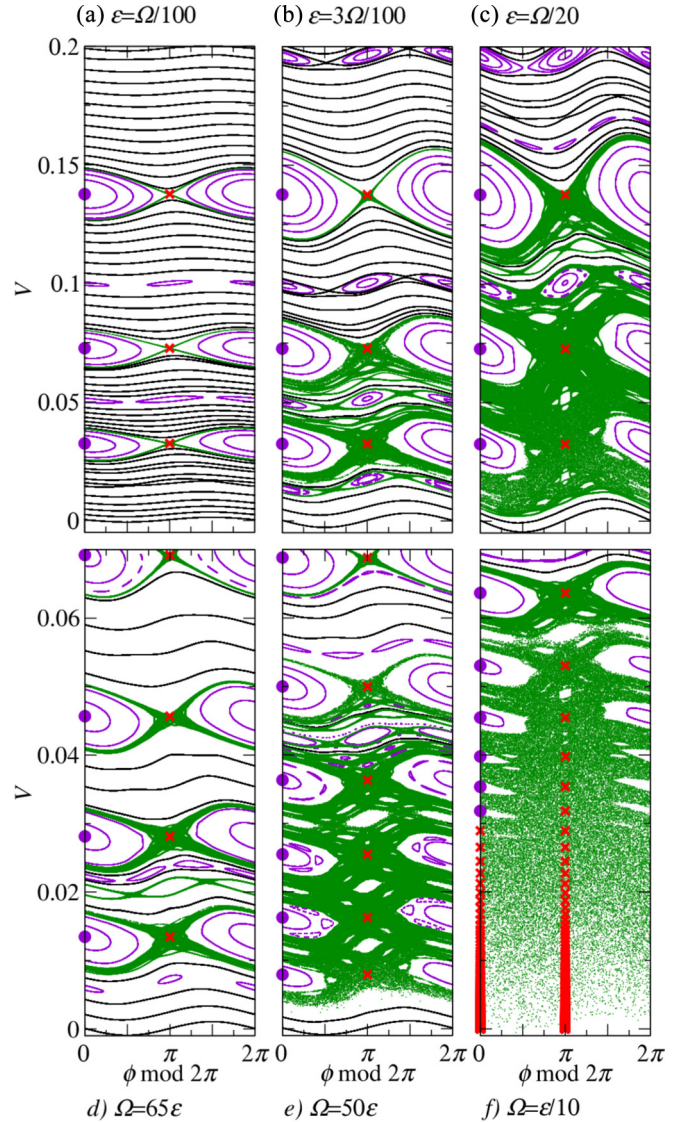


FIG. 3. The figure illustrates the phase space of the system for different combinations of values of parameters ϵ and Ω . In (a), (b), and (c) we used $\Omega = 10^{-1}$, and in (d), (e), and (f) we used $\epsilon = 10^{-3}$. The circles and the \times 's represent the locations of the fixed points.

atic motion. An example of such a situation is illustrated in Fig. 2(d). The collisions occur at distinct locations of the platform and the amplitude of the orbit of the particle changes in an irregular manner after each collision. Let us now discuss some aspects of the dynamics of the particle in the phase space.

III. PHASE SPACE

Figure 3 illustrates the phase space of the system for some combinations of parameters. In the top panels of Fig. 3 we show the changes of phase space when the parameter ϵ increases for $\Omega = 10^{-1}$. As we can see, for a fixed value of Ω and ϵ small enough, Fig. 3(a), the phase space is composed of periodic and quasiperiodic orbits, KAM islands around elliptical fixed points, and spanning curves. When the parameter ϵ increases, the separatrix curves at the lower portion

of phase space eventually became chaotic orbits. Further increases on ε lead the invariant curves close to these chaotic portions to dissolve and merge onto their neighbor chaotic portions, extending gradually the size of the chaotic components in phase space. Eventually, the development of two neighbor chaotic regions leads to a depletion of invariant spanning curves between them. Consequently, these chaotic pieces merge, giving rise to a broader component in phase space. To illustrate this phenomenon, we present in Fig. 3(b) the case where four chaotic portions are about to touch and in Fig. 3(c) we show a chaotic sea resulted from the blend between previously separated chaotic components.

In the bottom panels of Fig. 3 the amplitude of oscillation is $\varepsilon = 10^{-3}$ and the plots are displayed in a sequence where the ratio of frequencies, Ω , decreases. In Fig. 3(d) we see chaotic portions separated by invariant curves. As the parameter Ω decreases, invariant curves dissolve and the boundaries of the chaotic components expand. There are values of Ω for which chaotic portions merge and give rise to greater regions of chaotic behavior, Fig. 3(e). There is a limit for Ω below which the structure of the phase state does not change expressively. Figure 3(f) illustrates the asymptotic aspect of phase space for $\varepsilon = 10^{-3}$, when the value of Ω is small enough. We observe in Fig. 3(f) that an invariant spanning curve of lowest energy limits the size of the chaotic sea. In a limit of Ω small enough, the location of this invariant curve depends on ε and does not depend on Ω . Above this invariant curve there are other spanning curves with higher energy, elliptical fixed points surrounded by KAM islands, and small portions of chaotic motion. The existence of the spanning curves prevents the particle from acquiring arbitrary large values of energy, i.e., the system does not exhibit Fermi acceleration phenomenon. Moreover, if the particle is initially in the low energy portion of the phase space, these spanning curves ensure the existence of a finite value of radius of the sphere above which the motion of the particle is confined. An observation of the evolution of phase space as the parameters change suggests that ε and Ω affect the dynamics of the system in opposite ways in the sense where increasing ε for a fixed Ω promotes the rise and expansion of chaotic regions in phase space, while the same kind of development occurs when the parameter Ω decreases for a fixed ε .

As discussed before, a large value of the ratio of frequencies Ω can be regarded as a large amount of charge distributed in the sphere or a small frequency of oscillation of the platform. In both cases, after a collision the particle returns to a new collision and finds the platform at a position slightly different from the previous value. This process results in a condition where the motion of the particle is strongly correlated to the motion of the platform. In the opposite case, where Ω is small enough, in the time between two collisions the platform undertakes a large number of oscillations. This loss of correlation is responsible for introducing chaotic behavior in the dynamics of the particle. This mechanism occurs also in the Fermi-Ulam model.

To quantify the sensitivity of trajectories to initial conditions, we calculated the Lyapunov exponents associated to the chaotic component of phase space. Moreover, we used values of control parameters that correspond to the situations where the chaotic sea of the system occupies the portion of lowest

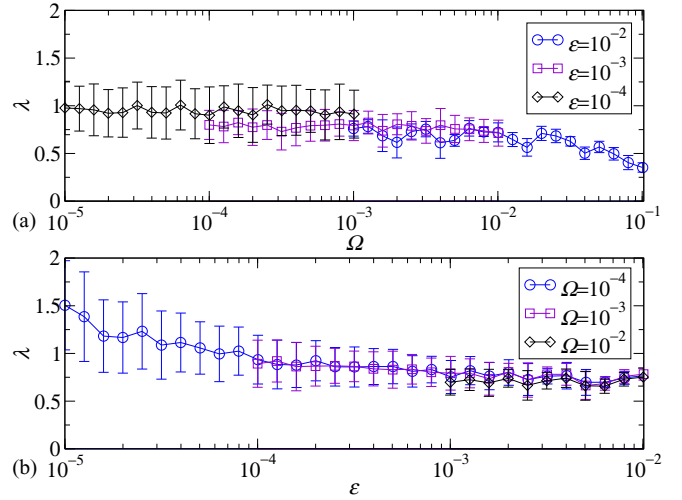


FIG. 4. Values of the greatest Lyapunov exponent (a) as a function of Ω for some values of ε , and (b) as a function of ε .

energy in phase space. We calculated the exponents using the triangulation procedure proposed by Eckmann and Ruelle [31]. This method consists in calculating the exponents λ_j , $j = 1, 2$, through the equation

$$\lambda_j = \lim_{n \rightarrow \infty} \frac{1}{n} \ln |\Lambda_j|, \quad (4)$$

where Λ_j are the eigenvalues of matrix $M = \prod_{i=1}^n J_i(V_i, \phi_i)$ and $J_i(V_i, \phi_i)$ is the Jacobian matrix evaluated over the orbit. The method furnishes a pair of Lyapunov exponents with opposite signals and, because the model under study does not present dissipation due to inelastic collisions, air resistance, friction, or electromagnetic radiation, the exponents have the same absolute value.

Figure 4(a) illustrates the values of the positive Lyapunov exponent when the parameter Ω changes for some values of ε . Each point corresponds to an average calculated from a hundred initial conditions where $V_0 = \varepsilon$ and ϕ_0 is randomly chosen in the interval $[0, 2\pi)$. This average is necessary because, although different orbits of a chaotic region have the same set of Lyapunov exponents, the limit in Eq. (4) is not achieved numerically and the Lyapunov exponents present fluctuations for a finite numbers of iterations.

Similarly, we display in Fig. 4(b) the positive Lyapunov exponent as a function of ε for some values of Ω . The standard deviation suggests the Lyapunov exponent fluctuates considerably. However, the average exponent does not change substantially over some decades of parameters ε and Ω . An average over all those values of Lyapunov exponents furnishes $\lambda = 0.8 \pm 0.2$.

We observe in Fig. 3 that chaotic orbits occur in the lowest energy portion of phase space when Ω is small enough. As previously discussed, there is a value of Ω below which the phase space remains approximately unchanged. In this regime, the size of the chaotic sea and the location of the invariant spanning curve with lowest energy depend only on parameter ε . We obtained an approximation for this curve through the following method. We divided the interval $\phi \in [0, 2\pi)$ into 10^4 strips of the same size. Each strip is

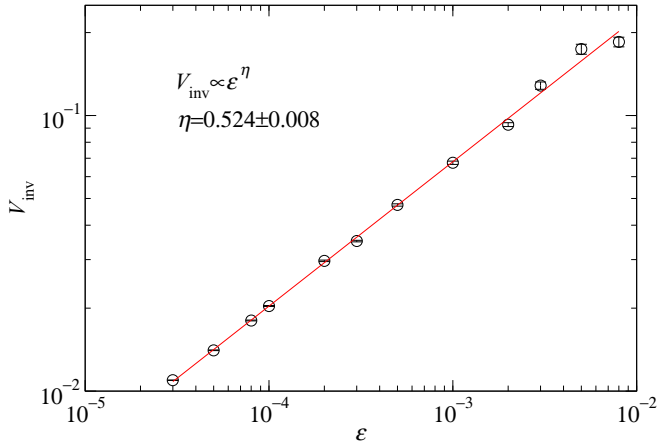


FIG. 5. Average velocity evaluated on the approximation to the lowest energy spanning curves as a function of ϵ .

associated to an element of an array. Initially we assign a small value of velocity, 10^{-6} , to all the elements of the array. Iterating the map given by Eq. (1) we obtain the orbit of an initial condition. After an iteration we obtain new values of phase and velocity. The value of phase obtained is located in a strip and, therefore, it is associated to an element of the array. If the value of velocity of the particle at this iteration is greater than the value of velocity stored in this element of the array, then the value of velocity in this element of the array is updated with the current value of velocity of the particle. Otherwise, the array remains unchanged. This process repeats for each new iteration of the map. As the trajectory evolves, the values of velocity gradually increase in each strip of phase and, for numbers of iterations large enough, this procedure furnishes a good approximation for the localization of the invariant curve with lowest energy. As a result, we obtain a curve in space V vs ϕ . This result becomes asymptotically close to the actual spanning curve as the number of iterations increases. Performing this procedure for different values of ϵ we obtain different curves as approximations to the corresponding spanning curves. Then we calculated the average value of velocity over each curve and we plotted this average velocity as a function of ϵ . We present in Fig. 5 the result of this approach. The best fit to the data furnishes $V_{inv} \propto \epsilon^\eta$ with $\eta = 0.524 \pm 0.008$.

In order to locate and classify the fixed points according to their stability, let us present a simplification of the model. The procedure we use is the same one that was employed previously by Holmes [7]. The simplified model consists in the approach where the time interval between two collisions is calculated regarding that the amplitude of oscillation of the moving platform is negligible. In this way we find that the time interval Δt_{n+1} between collisions is given by

$$\Omega \Delta t_{n+1} = \delta_n - \Omega t_n + \arccos(1/\rho_n) + 2\pi k, \quad (5)$$

where k is the smallest non-negative integer that ensures a positive value for Δt_{n+1} . The map that describes the simplified model is similar to the map in Eq. (1), where we must include absolute value bars to the velocity expression. The absolute value function is necessary in order to avoid the particle from going to the forbidden region $Y < 1 - \epsilon$. Moreover, we must

use $Y_n = 1$ in Eq. (2) and $\rho_n^2 = 1 + (V_n/\Omega)^2$. In this way, the simplification furnishes good approximation to the full model in the limit of small oscillations of the platform and for big values of velocity of the particle with relation to ϵ . The simplified model greatly decreases the time spent in the evaluation of the orbits of the particle because it exempts the simulations from the numerical solution of the transcendental equation (3).

It is worth mentioning that, depending on the parameter combinations, we observe some small regions of regular motion existing in the portion of low energy of phase space. In some of these situations the absolute value bars in the expression of velocity may introduce a chaotic trajectory into some of these small islands. Therefore, the simplified model presents some limitation and we must use it wisely. In this way the simplified model reproduces the main aspects of the full model, i.e., the same structure of KAM islands surrounded by a chaotic sea and invariant spanning curves observed in Fig. 3.

The fixed points are obtained solving the equations $V_{n+1} = V_n$ and $\phi_{n+1} \bmod 2\pi = \phi_n \bmod 2\pi$ simultaneously. After straightforward algebra we obtain the coordinates ϕ^* and V^* of the fixed points given below:

$$\begin{aligned} \phi^* &= 0, \pi, \\ V^* &= \Omega \tan(\pi m \Omega), \quad 0 < m < 1/(2\Omega). \end{aligned} \quad (6)$$

For each integer m that satisfies the inequality above, we have a value for V^* and both $\phi^* = 0$ and $\phi^* = \pi$. In the phase space of the full model, Fig. 3, we included the first fixed points obtained from Eq. (6) for the simplified model. These fixed points are represented with circles and \times 's. From the expressions above, we observe that, as the parameter Ω decreases, more fixed points are born, because more values of m become available. Moreover, those fixed points previously existing move downwards in phase space. In Fig. 3 we observe the increase in the number of fixed points in the low portion of phase space as Ω decreases.

To classify the fixed points according to their stability, we evaluate the eigenvalues of the Jacobian matrix

$$J = \begin{pmatrix} \frac{\partial V_{n+1}}{\partial V_n} & \frac{\partial V_{n+1}}{\partial \phi_n} \\ \frac{\partial \phi_{n+1}}{\partial V_n} & \frac{\partial \phi_{n+1}}{\partial \phi_n} \end{pmatrix}.$$

The eigenvalues have the form $\Lambda_{\phi^*}^\pm = [\text{tr } J \pm \sqrt{(\text{tr } J)^2 - 4 \det J}]/2$. Calculating the determinant of J we obtain $\det J = 1$, as a consequence of the preservation of area in phase space, and

$$\text{tr } J = 2 - \frac{4\epsilon}{\Omega^2} \cos^2(\pi m \Omega) \cos \phi^*. \quad (7)$$

Evaluating the eigenvalues explicitly, we find for the fixed points with $\phi^* = \pi$

$$\begin{aligned} \Lambda_\pi^\pm &= 1 + \frac{2}{\Omega} |\cos(\pi m \Omega)| \left[\frac{\epsilon}{\Omega} |\cos(\pi m \Omega)| \right. \\ &\quad \left. \pm \sqrt{\frac{\epsilon^2}{\Omega^2} \cos^2(\pi m \Omega) + \epsilon} \right]. \end{aligned} \quad (8)$$

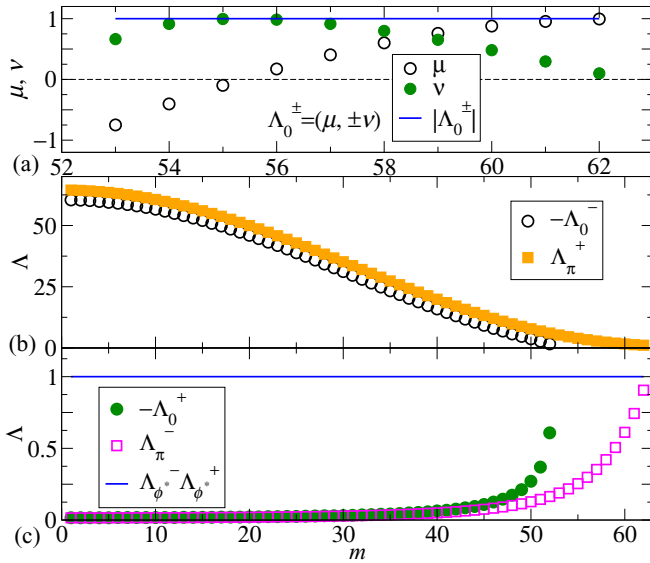


FIG. 6. (a) Real and imaginary parts of the eigenvalues associated to the elliptical fixed points with $\phi^* = 0$ as functions of m . The blue line corresponds to the absolute value of Λ_0^\pm . The plots (b) and (c) show the eigenvalues associated to the saddle points (ϕ^*, V^*) for both $\phi^* = 0$ and $\phi^* = \pi$. The blue line represents the product of the eigenvalues. The values of parameters are $\varepsilon = 10^{-3}$ and $\Omega = 8 \times 10^{-3}$.

We observe that the argument of the square root in the above equation is non-negative for all possible values of ε , Ω , and m . Then the eigenvalues Λ_π^\pm are real and, moreover, $\Lambda_\pi^- < 1$ and $\Lambda_\pi^+ > 1$. Therefore, the fixed points (π, V^*) are saddle points. Similarly, the eigenvalues for the fixed points with $\phi^* = 0$ are

$$\Lambda_0^\pm = 1 + \frac{2}{\Omega} |\cos(\pi m \Omega)| \left[-\frac{\varepsilon}{\Omega} |\cos(\pi m \Omega)| \pm \sqrt{\frac{\varepsilon^2}{\Omega^2} \cos^2(\pi m \Omega) - \varepsilon} \right]. \quad (9)$$

Depending on the values of ε , Ω , and m the argument of the square root in Eq. (9) is negative. It occurs when

$$\frac{1}{\pi \Omega} \arccos\left(\frac{\Omega}{\sqrt{\varepsilon}}\right) < m < \frac{1}{2\Omega}. \quad (10)$$

In these cases the eigenvalues are complex conjugate and the corresponding fixed points are classified as elliptical. In Fig. 6(a) we present the real and imaginary parts, μ and ν , respectively, of the eigenvalues associated to the elliptical fixed points $(0, V^*)$ as functions of m .

The fixed points $(0, V^*)$ are saddle points when the values of ε , Ω , and m satisfy the condition

$$m \leq \frac{1}{\pi \Omega} \arccos\left(\frac{\Omega}{\sqrt{\varepsilon}}\right). \quad (11)$$

The circles in Figs. 6(b) and 6(c) are associated to the eigenvalues Λ_0^- and Λ_0^+ of the fixed points with $\phi^* = 0$. The corresponding fixed points are saddle points because $|\Lambda_0^-| > 1$ and $|\Lambda_0^+| < 1$. The squares in Figs. 6(b) and 6(c)

represent the eigenvalues Λ_π^- and Λ_π^+ associated to the fixed points (π, V^*) , which are saddle points as discussed above. Moreover, we observe that the product of the eigenvalues is $\det J = 1$, as expected. The circles in Fig. 3 represent elliptical fixed points while the \times 's represent the saddle points. The simplified model furnishes a good approximation to the location of the fixed points and it is useful to classify these fixed points according to their stability in the full model.

The stability of the fixed points, especially those with $\phi^* = 0$, depends on both ε and Ω , Eq. (9). Moreover, Fig. 3 suggests that the location of fixed points does not depend on ε , and Eq. (6) confirms this observation. So, let us discuss how some aspects of the structure of fixed points in phase space develop when the ratio of frequencies, Ω , changes gradually. For a constant and arbitrary value of ε and increasing the value of Ω , the lowest fixed points $(0, V^*)$ in phase space, those corresponding to the first values of m , are saddle points [inequality (11)]. Moreover the fixed points $(0, V^*)$ at higher energies, associated to greater values of m , are elliptical [expression (10)]. In addition, the right size of the inequality (11) is a decreasing function on Ω . So, as Ω increases, all the fixed points move upwards in phase space [Eq. (6)], while the number of saddle fixed points with $\phi^* = 0$ decreases, because the highest saddle points with coordinate $\phi^* = 0$ become elliptical fixed points. Further increases in the value of Ω will eventually lead all fixed points at $\phi^* = 0$ to become elliptical. As previously mentioned, the total number of fixed points decreases as the parameter Ω grows. When it reaches the value $\Omega = 1/2$, the last pair of fixed points disappears [expressions (6)].

On the other hand, if we keep a constant value for Ω as the parameter ε increases, we have from inequality (11) that the number of saddle fixed points with $\phi^* = 0$ increases, while the number of elliptical fixed points decreases [inequality (10)]. In other words, the elliptical fixed points with lowest energy become saddle fixed points as ε increases.

Now that we have some knowledge about the behavior of individual trajectories in phase space, let us focus on the properties of ensembles of trajectories using average properties of chaotic orbits.

IV. AVERAGE PROPERTIES OF CHAOTIC SEA

Statistical physics is a branch of physics that is demonstrated to be successful when describing properties of different systems, ranging from magnetic materials [32] to interface growth [33] and biological interactions [34]. A classical example is the description of phase transition of water from liquid state to gaseous state in terms of scaling laws. To the best of our knowledge, the first scaling approach in dynamical systems was performed by Feigenbaum, when he studied the logistic map [35,36]. He described the route to chaos through period duplication using scaling functions characterized by two exponents. Feigenbaum developed a renormalization technique that allowed him to obtain the values of these exponents. Moreover, he demonstrated that the universality class is defined by the nonlinear term of lowest order in the function that describes the one-dimensional map. As we describe below, the dynamics of the system under study presents a transition and, similarly to the transitions

studied in statistical physics, this transition is characterized by scaling laws.

As described in the previous section, the size of chaotic portions depends on parameters ε and Ω . When the amplitude of motion of the platform is null, the velocity of the particle immediately after each collision is constant and the system is integrable. For $\varepsilon \neq 0$, however, the collisions with the moving platform introduce nonlinearity to the motion of the particle. In other words, the dynamical behavior of the system presents a transition from an integrable regime to a nonintegrable regime when the parameter ε changes from zero to a non-null value. So, near this transition, i.e., for $\varepsilon \approx 0$, it is expected that some properties of the bouncer model under study present invariance under scaling analysis.

For a fixed value of ε , the system does not present chaotic behavior in the limit of large values of Ω . Decreasing Ω leads small portions of chaos to arise at isolated locations of phase space. However, chaotic dynamics at the lowest energies emerges only below a value of Ω and, in this regime, the value of this parameter affects the phase space very weakly. In this section we discuss the universal properties of ensembles of trajectories with initial low energy that evolve in time in terms of scaling laws. We focus on the chaotic trajectories and, to ensure they have initial low energy, we employ $\Omega = \varepsilon/10$. Moreover, the results presented in this section were obtained for the complete model.

Firstly we define the average velocity of a trajectory j , obtained from a single initial condition, evaluated over the orbit according to

$$\langle V \rangle_j(n, \varepsilon, V_0) = \langle V \rangle_j = \frac{1}{n} \sum_{i=1}^n V_i.$$

Similarly, the average of the squared velocity is defined by

$$\langle V^2 \rangle_j(n, \varepsilon, V_0) = \langle V^2 \rangle_j = \frac{1}{n} \sum_{i=1}^n V_i^2.$$

Then we define the standard deviation of an ensemble of M initial conditions

$$\sigma(n, \varepsilon, V_0) = \frac{1}{M} \sum_{j=1}^M \sqrt{\langle V^2 \rangle_j - (\langle V \rangle_j)^2}.$$

This average over the ensemble corresponds to nonsimultaneous trajectories, in order to avoid electric interaction between multiple particles.

Figure 7 illustrates the standard deviation curves for different values of ε for the situations where the initial velocities are small, namely, $V_0 = \varepsilon/10$. The averages were obtained from $M = 10^4$ trajectories with initial phases $\phi_0 \in [0, \pi)$. We observe that each σ curve presents an initial power law growth regime. For values of n big enough, the standard deviation curves bend towards saturation values for all values of ε . Between the growth and saturation regimes there is, for each curve, a crossover value $n = n_x$.

We observe in Fig. 7 that for the limit $n \ll n_x$ the σ curves depend on ε and they grow as a power of n . In this limit we write the standard deviation as $\sigma(n \ll n_x, \varepsilon, V_0 \approx 0) = \sigma_{\text{grw}}$,

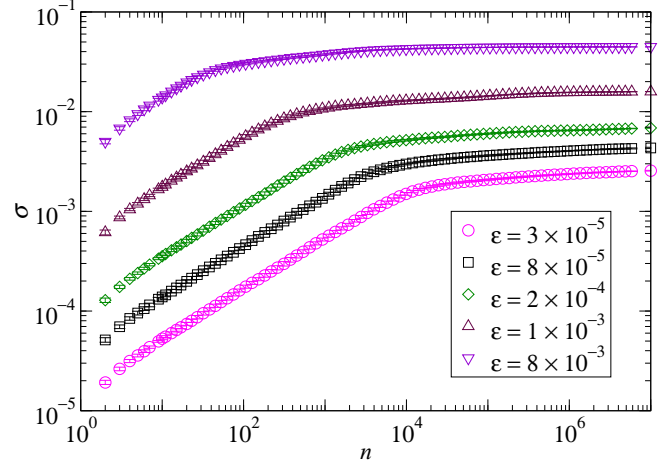


FIG. 7. Standard deviation of ensembles of trajectories with low initial velocities.

where

$$\sigma_{\text{grw}} \propto n^\beta \varepsilon^\gamma. \quad (12)$$

In this expression β is the growth exponent and γ is a critical exponent related to the dependence of σ on ε . Power law fittings to the growth regime of the standard deviation curves furnish the average value $\beta = 0.51 \pm 0.01$. The exponent γ was obtained from the plot of the average value of σ/n^β as a function of ε regarding the data corresponding to the growth regime. This procedure is illustrated in Fig. 8. The best fit to the numerical data furnishes $\gamma = 0.987 \pm 0.009$.

A close inspection of Fig. 7 in limit $n \gg n_x$ reveals the saturation regime is not culminated after 10^7 collisions. The saturation values of the standard deviation were obtained by extrapolating the numerical data in this limit. The asymptotic value $\sigma(n \gg n_x, \varepsilon, V_0 \approx 0)$, here represented by σ_{sat} , is given by the expression

$$\sigma_{\text{sat}} \propto \varepsilon^\alpha, \quad (13)$$

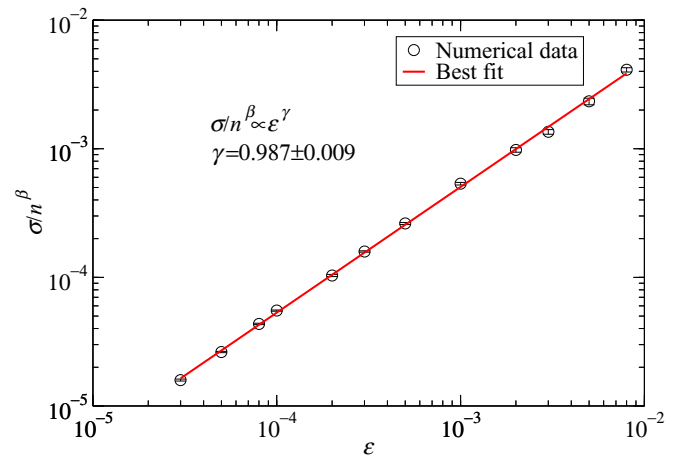


FIG. 8. The best fit to the data σ/n^β as a function of ε , represented by the red straight line, furnishes the exponent $\gamma = 0.987 \pm 0.009$ for $n \ll n_x$.

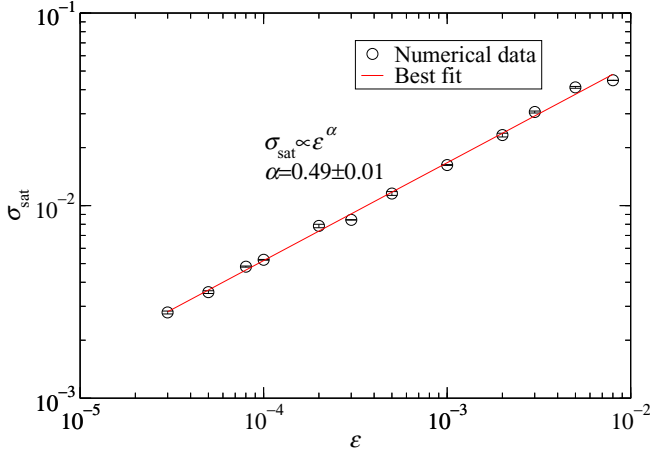


FIG. 9. Plot of saturation of the standard deviation as a function of ε . The nonlinear fit, illustrated by the red line, furnishes $\alpha = 0.49 \pm 0.01$.

where the critical exponent α that characterizes the saturation regime is called roughness exponent [33]. Figure 9 illustrates the plot of σ_{sat} for different values of ε . A power fit to the data furnishes the exponent $\alpha = 0.49 \pm 0.01$.

For the standard deviation curves in Fig. 7, the crossover from the growth regime to the saturation regime, n_x , is a function of ε and it is calculated by the equation

$$n_x = \left(\frac{\sigma_{\text{sat}}}{\kappa} \right)^{1/\beta},$$

where κ is the coefficient of the growth regime, which is obtained by a power law fitting for each value of ε . As shown in Fig. 10, the crossover n_x depends on ε as

$$n_x \propto \varepsilon^z, \quad (14)$$

where the dynamical exponent is $z = -0.99 \pm 0.02$.

The numerical evidences presented above suggest the standard deviation is described by a generalized homogeneous function with the following form:

$$\sigma(n, \varepsilon, V_0) = l\sigma(l^a n, l^b \varepsilon, l^c V_0). \quad (15)$$

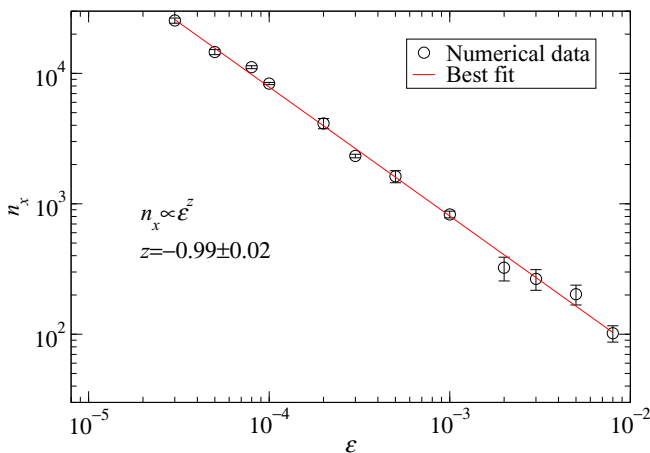


FIG. 10. Plot of the crossover value n_x as a function of ε . The best fit to the data furnishes $z = -0.99 \pm 0.02$.

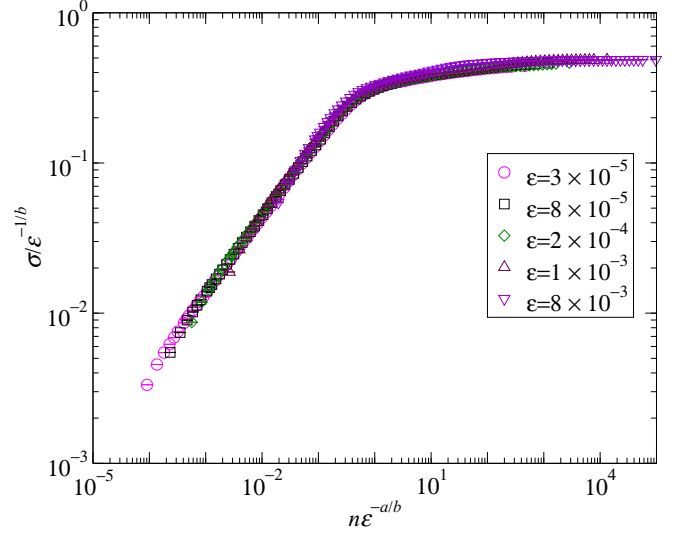


FIG. 11. The average standard deviation curves exhibit universal behavior under appropriated scaling transformations.

In this expression l is a scaling factor, and a , b , and c are scaling exponents. Choosing $l = \varepsilon^{-1/b}$ the above equation becomes

$$\sigma(n, \varepsilon, V_0) = \varepsilon^{-1/b} \sigma(\varepsilon^{-a/b} n, 1, \varepsilon^{-c/b} V_0). \quad (16)$$

For $V_0 \approx 0$ the above equation takes the form

$$\sigma(n, \varepsilon, V_0) \propto \varepsilon^{-(1+a\zeta)/b} n^\zeta. \quad (17)$$

Comparing this equation to (12) we obtain, for the growth regime, $\zeta = \beta$ and $a\beta + b\gamma = -1$. In the limit of large values of n we have, from Eqs. (13) and (17), $\zeta = 0$ and $b = -1/\alpha$. From Eq. (16) the crossover value of n is

$$n_x \propto \varepsilon^{a/b}. \quad (18)$$

Equations (14) and (18) furnish $z = a/b$. From these relations between the critical and the scaling exponents, and regarding the approximations $\alpha = \beta = 1/2$, $\gamma = 1$, and $z = -1$, we obtain $a = 2$ and $b = -2$. Performing the scaling transformations $n l^a$ and σ/l to the numerical data of Fig. 7, the universal behavior of the average standard deviation curves becomes evident, as shown in Fig. 11. The scaling factor used in this figure is $l = \varepsilon^{-1/b}$.

A way to obtain the value of the exponent c consists in using a result we present in Sec. III. In the limit of Ω small enough, the size of the chaotic sea, which is limited above by a lowest spanning curve, increases with ε according to $V_{\text{inv}} \propto \varepsilon^\eta$. From this equation we have $V_{\text{inv}}/\varepsilon^\eta = V'_{\text{inv}}/\varepsilon'^\eta = \text{constant}$, where $V'_{\text{inv}} = l^c V_{\text{inv}}$ and $\varepsilon' = l^b \varepsilon$. These relations lead to $c = b\eta = -1.07 \pm 0.04 \approx -1$.

The scaling arguments for the situations where $V_0 > \varepsilon$ are better illustrated in terms of the average velocity curves. In Fig. 12(a) we present some of these curves, some starting with $V_0 = \varepsilon/10$ and others with initial velocity $V'_0 > \varepsilon$ given by $V'_0 = l^c V_0$, where $l = (\varepsilon'/\varepsilon)^{1/b}$, $\varepsilon = 10^{-3}$, and $V_0 = 10\varepsilon$. The average velocity curves with $V_0 \approx 0$ are similar to the standard deviation curves σ presented in Fig. 7, i.e., they exhibit an initial growth regime followed by a saturation regime for large values of n , and the change from growth to saturation regime

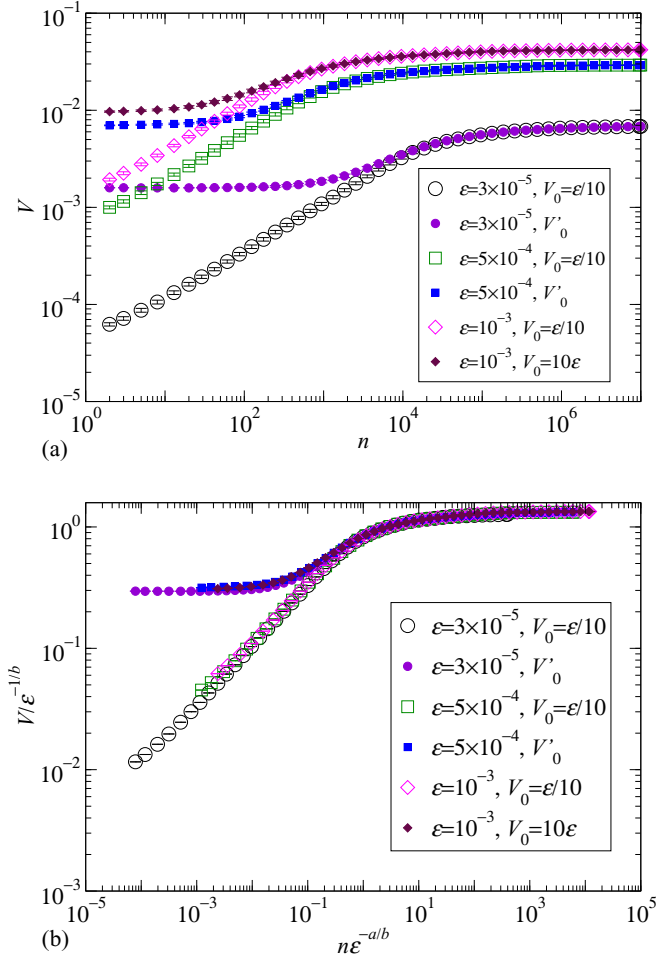


FIG. 12. (a) Some average velocity curves and (b) their universal behavior.

is characterized by a crossover n_x for each curve. On the other hand, the average velocity curves starting with $V_0 > \epsilon$ exhibit two crossover regimes. For $n \ll n'_x$ the curves present a regime where the values are approximately constant. Between n'_x and n''_x the V curves present growth regimes and they begin to follow the average velocity curves with $V_0 \approx 0$. For $n \gg n''_x$ each curve reaches a saturation regime that depends on ϵ and does not depend on V_0 . Moreover, n'_x goes to zero and n''_x goes to n_x in the limit where V_0 approximates to zero. Figure 12(b) displays the collapse of the average curves into a universal curve after appropriate scale transformations. It is important to mention that we use the same values of the scaling exponents a , b , and c obtained previously. Therefore, both σ and average velocities V are characterized by the same scaling description.

In the limit of Ω small enough the phase space of the system under study is not identical to the phase space of the Fermi-Ulam model [37] but they are very similar. In order to verify whether these two systems belong to a same class of universality, we change the dynamical variable n to $n\epsilon^2$. In this way we obtain the relation $2\beta = \gamma$ between critical exponents and the relations $b_2 = b$, $c_2 = c$, and $a_2 = a + 2b$, where a_2 , b_2 , and c_2 are the scaling exponents associated to the scaling description using the variable $n\epsilon^2$. Comparing these exponents to those presented in Ref. [38], we confirm that

the present model belongs to the class of universality of the Fermi-Ulam model.

V. DISCUSSIONS

Two main models considering particles colliding with walls recounting the idea of Fermi are the Fermi-Ulam model [10,30] and the bouncer model [7,26]. The first is composed of a classical particle colliding with two walls. One of them is fixed and the other one is periodically moving in time. The returning mechanism for a further collision with the moving wall is the fixed wall [12], where the particle collides and it is reflected backwards. The interval of time between two collisions is inversely proportional to the velocity of the particle. Therefore, the elapsed time between impacts is large for small velocities. This fact produces loss of correlation between the values of phase of the moving wall, leading to diffusion of velocity in the phase space [12]. As soon as the velocity of the particle increases due to the diffusion, correlated dynamics emerges leading to periodic islands. For velocities high enough, invariant spanning curves are observed. The invariant spanning curves work as barriers [10], not letting the particles cross through them. In this way, the lowest energy invariant spanning curve limits the size of the chaotic sea [38]. The scaling properties observed for the diffusion of particles in the chaotic sea strongly depend on the position of such a curve. The location of this lowest energy invariant spanning curve plays a major role in the dynamics [39], leading to the same set of critical exponents obtained in this paper.

On the other hand, in the bouncer model [6,13] the collisions happen with a single oscillating platform. The returning mechanism is a constant gravitational field [12]. As soon as the velocity of the particle increases, the interval of time between impacts increases as well, producing loss of correlation between the values of phase in the impacts. This process leads to unlimited diffusion of the velocity and, consequently, to Fermi acceleration [26]. The slope of the velocity growth depends on the dimensionless amplitude of oscillation of the platform. In this system, two main values of slope of growth of the velocity are observed: $1/2$, producing the normal diffusion, and 1 , leading to a fast regime of growth related to the accelerating modes.

There is also a hybrid Fermi-Ulam-bouncer model [40,41], which merges the two models into a single one. Depending on the values of amplitude of oscillation and intensity of the field, the particle experiences a competition between the dynamics produced by the Fermi-Ulam model and the bouncer model. Such a competition is characterized by a maximization of the Lyapunov exponent.

When the motion of the moving wall is described by a rather more complicated expression, such as a crank-connecting rod scheme [42], one of the parameters is the ratio between the radii of the crank and the length of the rod. In the limit where this ratio goes to unity, the moving wall may transfer large amounts of energy to the particle, and then, leading to unlimited energy growth.

Dissipative versions of both Fermi-Ulam, bouncer and hybrid versions were all considered. They present interesting phenomena such as boundary crisis [43,44], existence of shrimplike structures [45], cascades of period doubling

bifurcations that lead to the universality class of Feigenbaum's exponents [46], and many others.

Tufillaro *et al.* [47,48] presented the results of experimental realizations of the bouncer model. The authors found the boundaries between periodic orbits in parameter space, forcing frequency versus amplitude of oscillation, and they determined a way to obtain the restitution coefficient through the value of phase of platform at the bifurcation from the period-one to period-two transition [47]. In Ref. [48] the authors use a bouncing ball experiment in order to introduce undergraduate students to nonlinear phenomena in the laboratory. In this study, the students are instigated to find periodic and chaotic orbits by slowly changing the amplitude voltage of a function generator that drives the platform (a speaker). Wiesenfeld and Tufillaro [49] studied, both theoretically and experimentally, a process of period doubling suppression via periodic perturbations. They proposed a center manifold reduction in the vicinity of the first period doubling of the dissipative bouncer model and they found the normal form is the continuous-time limit of the second iterate of the reduced Poincaré return map. The experimental results show, in agreement with theoretical predictions, that decreasing the detuning enhances the suppression of period doubling. In an experimental realization of a bouncing ball, Mello and Tufillaro [50] showed some periodic orbits and the rising of strange attractors as the forcing amplitude of the speaker is increased. The results demonstrate excellent qualitative agreement when compared to the theoretical work developed by Holmes [7]. In Ref. [51] Tufillaro obtained a horseshoe template in standard form for the bouncer model, applied braid analysis to time series obtained from the bouncer model, and illustrated how measured braid invariants of the periodic orbits lead to the dynamical information about the flow. He showed also that the pruning methods used are systematic approximations in the sense that they generate an exact spectrum up to some period, beyond which lower bounds on the periodic orbit spectrum are provided. Vogel and Linz [52] studied a dissipative version of the bouncer model and they showed that chaotic motion, although present, does not dominate the parameter space and that, in the larger part of the parameter space, sticking motion prevails. They showed that both chaotic and periodic orbits coexist for some values of acceleration of the wall, restitution coefficient, and initial conditions. The authors investigated also the sticking solutions and the phenomenon of self-reanimating chaos. Moreover, the authors studied the scenario where the coefficient of restitution depends on velocity and they showed that the regions of chaotic and periodic solutions in parameter space grow. Langer and Miller [53] developed an investigation on the bouncer model where the motion of the platform is a piecewise linear function and the particle undergoes elastic and inelastic collisions. They studied the cases where the coefficient of restitution is constant and described by a function of velocity. For the situation where the coefficient of restitution is constant, the authors found that sticking trajectories where the particle experiences inelastic collapse was dominant. The authors showed that the sticking solutions are eliminated for the case where the coefficient of restitution is velocity dependent. In Ref. [54] the authors Huaraca and Mendoza described a method to obtain the minimal topological chaos associated to finite sets

of homoclinic and periodic orbits. Worrell *et al.* [55] investigated the dynamics of a particle whose velocity is continuous and the acceleration is discontinuous upon encountering the boundary. They showed the stochastic region is isolated by KAM surfaces and a new mechanism that segments the entire phase space into adjoining chaotic bands. They showed that the separatrix dividing each adjacent pair of bands consists of a continuous line of parabolic fixed points.

Lehtihet and Miller [56] studied a model of a mass point falling in a symmetric wedge. This system presents a rich variety of phenomena as the angle of wedge changes, and the authors analyzed some properties of global chaos that emerges in the system. Feldt and Olafsen [57] presented experimental results of a particle under gravity that collides against parabolic, wedge, and hyperbolic boundaries with horizontal motion. They found stable motion for the parabolic boundary and unstable motion for the wedge boundary. The authors obtained fractal behavior in the motion of the particle at low driving frequencies for hyperbolic boundary and irregular motion at higher driving frequencies. Hartl *et al.* [58] expanded the previous results presenting numerical simulations of a particle under acceleration of gravity in parabolic, wedge, and hyperbolic billiards. They showed that the particle exhibits stable periodic motion when colliding with parabolic boundary. For the situation where the boundary is hyperbolic, the authors showed that motion of the particle is regular for low driving frequencies, similarly to the results obtained for the parabolic boundary. They demonstrated that the motion of the particle is irregular for the wedge boundary and also for the hyperbolic boundary at high driving frequencies. The authors included in their modeling the rotational effects of the particle and additional forms of energy dissipation, namely, inelastic collisions, air resistance, and friction. Their results are in approximate agreement with the experimental data.

Two-dimensional billiards are a natural generalization of systems composed by particles that move in one dimension and collide against heavy walls. Depending on the shape of the boundary of the billiard, the particle exhibits regular dynamics [59], fully chaotic dynamics [60], or mixed structure [61]. Loskutov *et al.* [5] studied a two-dimensional Lorentz gas as a generalized kind of dispersing billiard. Moreover they considered the situations where the boundary of the system oscillates harmonically and stochastically. They showed that such a system presents Fermi acceleration and that the acceleration is higher for the situation where the boundary moves periodically. In Ref. [3] the authors showed that in stadiumlike billiards, for the developed chaos, the dependence of the particle velocity as a function of collisions number is similar to the Lorentz gas. They showed for a near-rectangle stadium billiard that, depending on initial conditions, the ensemble of particles presents Fermi acceleration or the velocity decreases to a quite low value. Moreover, the authors conjectured that a sufficient condition to achieve Fermi acceleration was the existence of chaotic orbits in phase space of the static version of the billiard, i.e., observation of positive Lyapunov exponents on a nontrivial region of phase space. Later, Lenz *et al.* [62] demonstrated for the time-dependent elliptical billiard that the driving leads to a layer of instability around the separatrix. It results in large fluctuations of the velocities of the particles as they cross it and, consequently, to Fermi

acceleration. Because the static elliptical billiard is an integrable system where the particle does not exhibit chaotic motion, the result presented by the authors allowed one to extend the previous conjecture. Shah *et al.* [63] studied a slitted rectangle where a particle collides elastically against the boundaries and against a horizontal bar that oscillates vertically. They showed the particle in this billiard presents, in average, exponential energy growth. Shah analyzed the rate of energy growth in the regime of large oscillations of the bar [64]. The author demonstrated that the energy growth rate of an ensemble of particles is lower than what is predicted by the log-normal distribution. Shah [65] showed also that large oscillations in chaotic billiards can result in a Fermi acceleration process greater than quadratic in time. Batistić [66] studied a generic billiard where the motion of fast variables is represented by a Markov model of transport between invariant orbits in the static versions of the billiards. The author demonstrated that if the number of possible paths through the space of invariant components grows exponentially in time, then exponential Fermi acceleration arises. Batistić studied also chaotic time-dependent shape-preserving billiards [67]. The theory is based on the study of the energy fluctuations in the adiabatic limit. The author demonstrated that the average velocity grows as a power of n , where the exponent is $1/6$ for the situation where a time-dependent transformation of billiard preserves the angular momentum, and the exponent is $1/4$ otherwise. Lens *et al.* [68] showed for three different driving modes in the elliptical billiard that Fermi acceleration is achieved. They obtained subdiffusive transport in momentum space for the constant eccentricity mode and, for the breathing and quadrupole modes, they observed a crossover from subdiffusion to normal diffusion.

Depending on the combinations of values of platform amplitude and initial conditions, Fermi acceleration is observed in the bouncer model with homogeneous gravitational field. However, for the nonhomogeneous field presented here, the numerical simulations suggest that Fermi acceleration is not achieved, since the presence of spanning curves limit the diffusion of trajectories in phase space. Although this numerical evidence, analytical results are still needed to prove convincingly the absence of Fermi acceleration.

In the present model, the returning mechanism of the particle is a nonhomogeneous field. A restoring force conducts the particle back to the moving platform for a next collision. We notice that the scaling properties observed for the chaotic diffusion resemble the characteristics observed in the Fermi-Ulam model since the presence of the invariant spanning curves limits the diffusion of the particles. Even though the returning mechanism for the model discussed in this paper depends on the ratio of frequencies, Ω , and V_n , the critical dynamics showing the scaling for the diffusion of the chaotic orbits produces a set of critical exponents identical to those observed on the Fermi-Ulam model. Hence the dynamics of the present system has critical properties belonging to the same universality class as the Fermi-Ulam model. The scaling approach allows us to conclude that these different systems present chaotic seas with the same fundamental dynamical behavior in the limit where Ω is small enough and, therefore, to move forward to a better characterization of the diffusion and scaling invariance of the chaotic dynamics. Moreover, the

framework discussed here allows one to extend the procedure to another far complex system such as magnetic billiards with time moving boundaries.

VI. CONCLUSIONS

We conducted a study in a model where a charged particle is accelerated due to the electric force inside a sphere with homogeneous charge distribution. The particle collides elastically against a moving platform and the impacts introduce nonlinearity to the motion of the particle. This is so far a specific example of a one-dimensional billiard experiencing elastic collisions and a linear restoring force. The dynamics of the particle is controlled by two parameters: a ratio of frequencies Ω and the dimensionless amplitude of oscillation ε . For a fixed value of Ω , chaotic motion of the particle eventually becomes evident as the nonlinearity strength ε increases. On the other hand, for a fixed value of ε , the size of chaotic regions in phase space increases as the parameter Ω decreases. Chaotic dynamics arises when, in the time interval between collisions, loss of correlation between the motion of the particle and the motion of the platform occurs. We use a simplified model (static wall approximation) to obtain the location of the fixed points and classify them according to their stability. Different from the Fermi-Ulam model, the location of the fixed points does not depend on the nonlinearity parameter. We discuss how the structure of fixed points in phase space develops as the parameters ε and Ω change gradually. In the second part of the paper we study some average properties of the chaotic sea in the limit of Ω small enough, where the lowest energy chaotic sea is approximately independent on Ω . We show that, near the transition from the integrable to the nonintegrable regimes, $\varepsilon \approx 0$, the system presents scaling invariance and it belongs to the class of universality of the Fermi-Ulam model. The model under investigation and the results here presented serve to motivate further studies and, perhaps, experimental approaches.

ACKNOWLEDGMENTS

F.A.O.S. thanks FAPEMIG for the financial support. D.G.L. and S.G.A. acknowledge CNPq, FAPEMIG, and CAPES. E.D.L. acknowledges support from CNPq (301318/2019-0) and FAPESP (2019/14038-6). CAPES, CNPq, FAPEMIG and FAPESP are Brazilian agencies.

APPENDIX

In this section we describe the details that lead to Eqs. (1), (2), and (3). Let us suppose that at the instant of collision n , t'_n , the position of the particle is $y(t'_n) = y_n$ and its velocity is $v(t'_n) = v_n$. The value of y_n is given by the position of the platform at instant t'_n , i.e., $y_p(t'_n) = \ell_0 + \varepsilon \cos(\omega t'_n + \phi_0)$. From the second Newton's law, the motion of the particle is described by the differential equation $d^2y/dt'^2 = -\omega_f^2 y$, where $\omega_f^2 = q_0 Q / (4\pi \varepsilon_0 R^3 m)$. The solution of the differential equation is $y(t') = o'_n \cos(\omega_f t') + p'_n \sin(\omega_f t')$, where o'_n and p'_n are constants between the collisions n and $n + 1$. The values of o'_n and p'_n are determined from the initial conditions

y_n and v_n by the equations

$$\begin{aligned} o'_n &= y_n \cos(\omega_f t'_n) - (v_n/\omega_f) \sin(\omega_f t'_n), \\ p'_n &= y_n \sin(\omega_f t'_n) + (v_n/\omega_f) \cos(\omega_f t'_n). \end{aligned} \quad (\text{A1})$$

Defining the new variables q_n and δ_n through the equations $o'_n = q_n \cos \delta_n$ and $p'_n = q_n \sin \delta_n$, we obtain an alternative expression for the position of the particle given by $y(t') = q_n \cos(\omega_f t' - \delta_n)$, with $q_n^2 = o_n'^2 + p_n'^2 = y_n^2 + (v_n/\omega_f)^2$.

Immediately before the collision $n+1$ the particle has velocity $v^- = -q_n \omega_f \sin(\omega_f t'_{n+1} - \delta_n)$ and the platform has velocity $\mathcal{V}^- = -\epsilon \omega \sin(\omega t'_{n+1} + \phi_0)$. In the referential of the platform the velocity of the particle is given by $v'^- = v^- - \mathcal{V}^-$. The collision is elastic. Therefore, in the referential of the platform, the velocity of the particle changes the signal preserving the absolute value. Then, immediately after the collision $n+1$, the velocity of the particle is given by $v'^+ = q_n \omega_f \sin(\omega_f t'_{n+1} - \delta_n) - \epsilon \omega \sin(\omega t'_{n+1} + \phi_0)$. Changing to the referential of the laboratory, the velocity of the particle immediately after the collision $n+1$ is given by

$$\begin{aligned} v_{n+1} &= q_n \omega_f \sin(\omega_f t'_{n+1} - \delta_n) \\ &\quad - 2\epsilon \omega \sin(\omega t'_{n+1} + \phi_0). \end{aligned} \quad (\text{A2})$$

Dividing both sides of Eq. (A2) by $\omega \ell_0$, using the dimensionless time $t = \omega t'$ and the relations $\rho_n = q_n/\ell_0$, $\phi = t + \phi_0$, $\varepsilon = \epsilon/\ell_0$, $\Omega = \omega_f/\omega$, and $V = v/(\omega \ell_0)$, we obtain the dimensionless velocity expression V_{n+1} in Eq. (1).

The instant of collision $n+1$ is given by $t'_{n+1} = t'_n + \Delta t'_{n+1}$, where $\Delta t'_{n+1}$ is the time interval between the collisions n and $n+1$. Multiplying both sides of this equation by ω , adding ϕ_0 to both sides and using the expressions $t = \omega t'$ and $\phi_n = t_n + \phi_0$ we obtain the expression for ϕ_{n+1} in Eq. (1).

The collision $n+1$ occurs when the particle reaches the platform at instant t'_{n+1} , i.e., $y(t'_{n+1}) - y_p(t'_{n+1}) = 0$. Using the position expressions of the particle and the platform, this equation becomes

$$\begin{aligned} o'_n \cos(\omega_f t'_{n+1}) + p'_n \sin(\omega_f t'_{n+1}) \\ - \ell_0 - \epsilon \cos(\omega t'_{n+1} + \phi_0) = 0. \end{aligned} \quad (\text{A3})$$

Now we divide both sides of above equation by ℓ_0 , and we use the expression $t' = t/\omega$ and the dimensionless quantities $\Omega = \omega_f/\omega$, $\varepsilon = \epsilon/\ell_0$, and $t_{n+1} = t_n + \Delta t_{n+1}$. With this procedure Eq. (A3) becomes Eq. (3) with $o_n = o'_n/\ell_0$ and $p_n = p'_n/\ell_0$. We obtain the expressions of o_n and p_n in Eq. (2) using the definitions $Y = y/\ell_0$ and $t_n = \phi_n - \phi_0$ in Eqs. (A1).

-
- [1] V. Gelfreich and D. Turaev, *Commun. Math. Phys.* **283**, 769 (2008).
- [2] J. Koiller, R. Markarian, S. O. Kamphorst, and S. P. de Carvalho, *Nonlinearity* **8**, 983 (1995).
- [3] A. Loskutov, A. B. Ryabov, and L. G. Akinshin, *J. Phys. A: Math. Gen.* **33**, 7973 (2000).
- [4] N. Chernov and R. Markarian, *Chaotic Billiards*, Mathematical Surveys and Monographs Vol. 127 (American Mathematical Society, Providence, RI, 2006).
- [5] A. Loskutov, A. B. Ryabov, and L. G. Akinshin, *J. Exp. Theor. Phys.* **89**, 966 (1999).
- [6] L. D. Pustynnikov, *Trans. Moscow Math. Soc.* **2**, 1 (1978).
- [7] P. J. Holmes, *J. Sound Vib.* **84**, 173 (1982).
- [8] F. Saif, *Phys. Rep.* **419**, 207 (2005).
- [9] F. Saif, *Phys. Rep.* **425**, 369 (2006).
- [10] A. J. Lichtenberg, M. A. Lieberman, and R. H. Cohen, *Physica D* **1**, 291 (1980).
- [11] B. V. Chirikov, *Phys. Rep.* **52**, 263 (1979).
- [12] A. J. Lichtenberg and M. A. Lieberman, *Regular and Chaotic Dynamics*, Applied Mathematical Sciences Vol. 38 (Springer-Verlag, New York, 1992).
- [13] R. M. Everson, *Physica D* **19**, 355 (1986).
- [14] P. Pieranski, *J. Phys. (Paris)* **44**, 573 (1983).
- [15] M. Franaszek and P. Pieranski, *Can. J. Phys.* **63**, 488 (1985).
- [16] Z. J. Kowalik, M. Franaszek, and P. Pieranski, *Phys. Rev. A* **37**, 4016 (1988).
- [17] Wen-Yu Chen and G. J. Milburn, *Phys. Rev. E* **56**, 351 (1997).
- [18] S. T. Dembiński, A. J. Makowski, and P. Peplowski, *Phys. Rev. Lett.* **70**, 1093 (1993).
- [19] J.-C. Géminard and C. Laroche, *Phys. Rev. E* **68**, 031305 (2003).
- [20] F. Pacheco-Vázquez, F. Ludewig, and S. Dorbolo, *Phys. Rev. Lett.* **113**, 118001 (2014).
- [21] D. G. Ladeira and J. K. L. da Silva, *J. Phys. A: Math. Theor.* **40**, 11467 (2007).
- [22] N. A. Burnham, A. J. Kulik, G. Gremaud, and G. A. D. Briggs, *Phys. Rev. Lett.* **74**, 5092 (1995).
- [23] A. L. P. Livorati, I. L. Caldas, C. P. Dettmann, and E. D. Leonel, *Phys. Lett. A* **379**, 2830 (2015).
- [24] A. C. J. Luo and R. P. S. Han, *Nonlinear Dyn.* **10**, 1 (1996).
- [25] J. J. Barroso, M. V. Carneiro, and E. E. N. Macau, *Phys. Rev. E* **79**, 026206 (2009).
- [26] A. L. P. Livorati, T. Kroetz, C. P. Dettmann, I. L. Caldas, and E. D. Leonel, *Phys. Rev. E* **97**, 032205 (2018).
- [27] Y. Couder, S. Protiere, E. Fort, and A. Boudaoud, *Nature (London)* **437**, 208 (2005).
- [28] E. D. Leonel and A. L. P. Livorati, *Commun. Nonlinear Sci. Numer. Simul.* **20**, 159 (2015).
- [29] L. Mátyás and R. Klages, *Physica D* **187**, 165 (2004).
- [30] A. K. Karlis, P. K. Papachristou, F. K. Diakonou, V. Constantoudis, and P. Schmelcher, *Phys. Rev. Lett.* **97**, 194102 (2006).
- [31] J. P. Eckmann and D. Ruelle, *Rev. Mod. Phys.* **57**, 617 (1985).
- [32] F. Reif, *Fundamentals of Statistical and Thermal Physics* (Waveland Press, Long Grove, IL 2009).
- [33] A.-L. Barabási and H. E. Stanley, *Fractal Concepts in Surface Growth* (Cambridge University Press, Cambridge, 1995).
- [34] M. M. de Oliveira and R. Dickman, *Phys. Rev. E* **90**, 032120 (2014).
- [35] M. J. Feigenbaum, *J. Stat. Phys.* **19**, 25 (1978).
- [36] M. J. Feigenbaum, *J. Stat. Phys.* **21**, 669 (1979).
- [37] E. D. Leonel, J. K. L. da Silva, and S. O. Kamphorst, *Physica A* **331**, 435 (2004).
- [38] E. D. Leonel, P. V. E. McClintock, and J. K. L. da Silva, *Phys. Rev. Lett.* **93**, 014101 (2004).
- [39] E. D. Leonel, J. A. de Oliveira, and F. Saif, *J. Phys. A: Math. Theor.* **44**, 302001 (2011).

- [40] E. D. Leonel and P. V. E. McClintock, *J. Phys. A: Math. Gen.* **38**, 823 (2005).
- [41] D. G. Ladeira and E. D. Leonel, *Chaos* **17**, 013119 (2007).
- [42] E. D. Leonel and M. R. Silva, *J. Phys. A: Math. Theor.* **41**, 015104 (2007).
- [43] E. D. Leonel and P. V. E. McClintock, *J. Phys. A: Math. Gen.* **38**, L425 (2005).
- [44] E. D. Leonel and R. E. de Carvalho, *Phys. Lett. A* **364**, 475 (2007).
- [45] D. F. M. Oliveira and E. D. Leonel, *New J. Phys.* **13**, 123012 (2011).
- [46] D. F. M. Oliveira and E. D. Leonel, *Braz. J. Phys.* **38**, 62 (2008).
- [47] N. B. Tufillaro, T. M. Mello, Y. M. Choi, and A. M. Albano, *J. Phys.* **47**, 1477 (1986).
- [48] N. B. Tufillaro and A. M. Albano, *Am. J. Phys.* **54**, 939 (1986).
- [49] K. Wiesenfeld and N. B. Tufillaro, *Physica D* **26**, 321 (1987).
- [50] T. M. Mello and N. B. Tufillaro, *Am. J. Phys.* **55**, 316 (1987).
- [51] N. B. Tufillaro, *Phys. Rev. E* **50**, 4509 (1994).
- [52] S. Vogel and S. J. Linz, *Int. J. Bifurcation Chaos* **21**, 869 (2011).
- [53] C. K. Langer and B. N. Miller, *Chaos* **25**, 073114 (2015).
- [54] W. Huaraca and V. Mendoza, *Physica D* **315**, 83 (2016).
- [55] G. A. Worrell, A. Matulich, and B. N. Miller, *Chaos* **3**, 397 (1993).
- [56] H. E. Lehtihet and B. N. Miller, *Physica D* **21**, 93 (1986).
- [57] S. Feldt and J. S. Olafsen, *Phys. Rev. Lett.* **94**, 224102 (2005).
- [58] A. E. Hartl, B. N. Miller, and A. P. Mazzoleni, *Phys. Rev. E* **87**, 032901 (2013).
- [59] N. Chernov and R. Markarian, *Chaotic Billiards* (American Mathematical Society, Providence, RI, 2006), Vol. 127.
- [60] L. A. Bunimovich, *Commun. Math. Phys.* **65**, 295 (1979).
- [61] M. V. Berry, *Eur. J. Phys.* **2**, 91 (1981).
- [62] F. Lenz, F. K. Diakonov, and P. Schmelcher, *Phys. Rev. Lett.* **100**, 014103 (2008).
- [63] K. Shah, D. Turaev, and V. Rom-Kedar, *Phys. Rev. E* **81**, 056205 (2010).
- [64] K. Shah, *Phys. Rev. E* **88**, 024902 (2013).
- [65] K. Shah, *Phys. Rev. E* **83**, 046215 (2011).
- [66] B. Batistić, *Phys. Rev. E* **90**, 032909 (2014).
- [67] B. Batistić, *Phys. Rev. E* **89**, 022912 (2014).
- [68] F. Lenz, C. Petri, F. K. Diakonov, and P. Schmelcher, *Phys. Rev. E* **82**, 016206 (2010).